Mineralogy and Geochemistry of the High-Cr Podiform Chromitite from the Cuobuzha Ophiolite, Yarlung Zangbo Suture Zone, Western Tibet, China: Implication for its Origin

GSC

ZHAO Hui[1, 2, 3], YANG Jingsui[3, 4, *], LIU Fei[3], XIONG Fahui[3], LIAN Dongyang[4] and YAO Hu[5]

[1] *Harbin Institute of Technology, Harbin 150001, China.*

[2] *Department of Earth and Space Sciences, Southern University of Science and Technology, Shenzhen 518055, China*

[3] *Institute of Geology, Chinese Academy of Geological Sciences, Beijing 100037, China*

[4] *School of Earth Sciences and Engineering, Nanjing University, Nanjing 201123, China*

[5] *Institute of Geochemistry Chinese Academy of Sciences, Guiyang 550081, China*

Abstract: The Cuobuzha high-Cr chromitites in the western segment of Yarlung Zangbo Suture Zone of Tibet are mainly hosted in the harzburgites as massive type, which are characterized by high concentrations of platinum group elements (PGE) ranging from 380 to 577 ppb, and low Pd/Ir ratios (<0.1). In mid-ocean ridge basalts (MORB)-normalized spidergrams, chromites of the Cuobuzha chromitites are depleted in Al, Ga, V, Mg and Zn, and enriched in Mn and Cr, sharing similar patterns with those of ophiolitic boninites in the Bonin and Thetford Mines. Approximately 20 platinum group mineral (PGM) grains were discovered from the samples, including laurite, erlichmanite, Os-Fe alloy, cuproiridsite, and irarsite. The PGM assemblages indicate that sulfur fugacity was initially low enough to allow the precipitation of Os-Fe alloy and increased thereafter, with the fall in temperature. Primary Fe-Ni and Fe-Cr alloys, which are stable in a highly reduced environment, occur as inclusions within chromites or clinopyroxenes. Calculated results show that the parental magma has an intimate affinity with boninites. Based on our observations, a model is proposed wherein the Cuobuzha chromitites contain high-pressure and low-pressure chromites. Low-pressure chromites were formed via reaction between boninitic melts and peridotites, during which the high-pressure chromites hosting highly reduced minerals were mobilized by melts and were reallocated to podiform chromitites.

Key words: Cuobuzha chromitites, highly reduced minerals, Yarlung Zangbo Suture Zone, Tibet

1 Introduction

Podiform chromitites, which are typical of ophiolites, are considered as important economic sources for chromium which is one of the strategic metals used for industrial production (Leblanc et al., 1992). These lens-shaped orebodies vary from a few kilograms to a few million tons and are hosted in depleted peridotites less than 500 m below the petrologic Moho (Leblanc et al., 1992; Zhou et al., 2014).

The genesis of podiform chromitites has long been a matter of debate. Early works suggested that fractional crystallization of basaltic melts in magma chambers or conduits in the upper mantle resulted in the formation of podiform chromitites (Thayer, 1964; Dickey, 1975; Cassard et al., 1981; Lago et al., 1982; Leblanc et al., 1992). A later model suggested that these chromitites were the residuals after a large amount of melts had been extracted from the primitive mantle (Wang et al., 1992; Bao et al., 1999). Modeling experiments have demonstrated that partial melting of the upper mantle not

only can influence the evolution of mantle rocks (lherzolite→harzburgite→dunite), but also can play an important role in preconcentration of chromites (Jin et al., 1996). Kelemen et al. (1992) proposed that melt/rock reaction was prevalent in the upper mantle, which was testified by some peridotite samples with high SiO_2 and light rare earth elements (LREE) contents in this region. Since then, the idea that podiform chromitites are formed through reaction between mantle peridotites (especially harzburgites) and boninitic or tholeiitic melts has attracted considerable attention from many scholars (Arai and Yurimoto, 1994; Zhou et al., 1994, 1996, 1997; Arai, 1997; Edwards et al., 2000; Rollinson and Adetunji, 2013; Arai et al., 2015). However, occurrence of ultrahigh pressure (UHP) and highly reduced minerals (e.g., diamond and moissanite) strongly suggests that podiform chromitites are formed at mantle depths of 150–300 km or even greater (Yang et al., 1981; Bai et al., 2001, 2002, 2004, 2007; Yang et al., 2002, 2007, 2011, 2013, 2014, 2015a, b; Xu et al., 2008, 2009, 2013, 2015).

Although there are a number of studies on podiform chromitites so far, the tectonic settings for them are still unclear (Arai and Matsukage, 1998; Pearce et al., 1984;

* Corresponding author. E-mail: yangjsui@163.com

Zhou and Robinson, 1994, 1997; Rollinson and Adetunji, 2013). Nicolas et al. (1989) proposed that podiform chromitites were formed in a mid-ocean ridge setting based on their occurrences and structures. Furthermore, chromitite micropods, which are similar to alpine-type chromitite pods, were recovered from the Hess Deep of the equatorial Pacific, directly demonstrating that podiform chromitites could form at fast-spreading ridge environments (Arai and Matsukage, 1998). However, nowadays many scientists consider suprasubduction zone as a more suitable setting for podiform chromitites (Pearce et al., 1984; Zhou and Robinson, 1994, 1997; Rollinson and Adetunji, 2013). Chromitite xenoliths from the Takashima alkaline basalt in the southwest Japan arc favor the existence of chromitite beneath arcs (Arai and Abe, 1994).

Yarlung Zangbo Suture Zone (YZSZ) contains abundant chromite deposits; more than 80% of chromite ores in China occur in this belt (Hang et al., 2006, 2007). Majority of the studies thus far have focused on the Luobusha ophiolite occurring in the eastern part of this belt, which contains the largest chromite deposit in China (Zhou et al., 1996, 2005; Bao et al., 1999; Bai et al., 2004, 2007; Yamamoto et al., 2009; Xiong et al., 2015; Xu et al., 2015). In recent years, some studies have reported considerable chromite deposits in the western segment of YZSZ, such as Dongbo, Purang, Dangqiong ophiolite massifs (Huang et al., 2006, 2007; Yang et al., 2011; Xiong et al., 2011, 2016; Xu et al., 2011). However, the studies are few owing to the inhospitable working conditions. The Cuobuzha ophiolite, which hosts massive chromitites, is located in this segment (Zhao et al., 2019). In this study, we carried out detailed mineralogical and geochemical investigations on the chromitites in Cuobuzha to determine the origin of podiform chromitites.

2 Regional Geology

The Tibetan Plateau is a collage of continental fragments with intervening suture zones (Fig. 1b). The YZSZ is the southernmost and youngest suture zone in the Tibetan Plateau, which separates the Lhasa terrane in the north and the Indian Plate in the south. It mainly consists of nearly continuous, but tectonically disrupted east–west trending ophiolites, which represent the remnants of the Neo-Tethys Ocean (Aitchison et al., 2007; Dilek and Furnes, 2011, 2014; Hébert et al., 2012). Based on their spatial distribution, ophiolites within the YZSZ are divided into three parts: the east (Qu Shui to Mo Tuo), the middle (Ang Ren to Ren Bu) and the west (Saga to the Sino–Indian border) (Zhang et al., 2011). The western part includes the Dajiweng–Saga ophiolite sub-belt in the north (NSB) and the Daba–Xiugugabu ophiolite sub-belt in the south (SSB) (Fig. 1c). These two sub-belts are separated by the 60 km wide Zhada–Zhongba micro-continental block, which mainly consists of discontinuous Sinian–Cambrain metamorphic rocks and Ordovician–Triassic marine strata (Pan et al., 1997; Huang et al., 2006, 2007; Xu et al., 2006, 2007; Li et al., 2014; Liu et al., 2015a). Ophiolites in the NSB are small in size (~10 km long and 1–2 km wide) and crop out discontinuously. They are

mainly composed of serpentinized peridotites, gabbro, dolerite dykes, basaltic lavas and chert. Fresh peridotite massifs mainly occur, from west to east, in Dajiweng, Baer, Kazhan, Cuobuzha, Zhalai, Gongzhu, and Saga (Xia et al., 1995, 1997; Li et al., 2011; Feng et al., 2015, 2016; Lian et al., 2015; Liu et al., 2013, 2015a, b). The ophiolite massifs in the SSB mainly include the Dongbo (400 km^2), Purang (650 km^2), Dangqiong (440 km^2) and Xiugugabu (260 km^2) complexes, which are larger than those in the NBS (Huang et al., 2006, 2007; Bédard et al., 2009; Yang et al., 2011; Xiong et al., 2011; Xu et al., 2011; Liu et al., 2013, 2015a, b).

The Cuobuzha ophiolite is located in the NSB and is emplaced onto the Gangdese Batholith which is exposed along the southern margin of the Lhasa terrane. In the south, the Cuobuzha ophiolite is separated from the Jurassic–Cretaceous tectonic mélange by a major fault (Fig. 2).

3 Field Occurrence and Petrology

The ophiolitic sequence in Cuobuzha is dismembered, which mainly consists of peridotites and dolerite dykes (Fig. 3). The peridotite massif is 0.2 to 0.5 km in width and 3 to 5 km in length, tectonically overlaid by listwanite, and is dominantly composed of harzburgites with minor amounts of lherzolites and dunites. The fresh harzburgites are dark green and coarse-grained, and chiefly comprise of olivines (50% –55%) and orthopyroxenes (35% –45%), and lesser amounts of clinopyroxenes (2% – 5%) and chromian spinels (2%–5%). Geochemical characteristics of the Cuobuzha harzburgites suggest that they were originally formed at a mid-oceanic spreading ridge and were later modified by fluids and melts in suprasubduction zone (SSZ) (Feng et al., 2015, 2016). Dolerite dykes cutting into harzburgites yielded zircon U-Pb ages of 130–125 Ma (Liu et al., 2015b).

Massive chromitites are hosted in harzburgites with rare dunite shells. The orebodies are approximately 0.5–1 m thick and typically comprise of more than 90 modal% magnesiochromites, which are usually brecciated. The spaces between cracked magnesiochromite crystals are generally filled with chlorites/serpentines. Almost all the samples are composed of fresh magnesiochromite crystals. However, in some cases, alteration was also significant along the margins and fractures of the crystals (Fig. 4). The composition of magnesiochromites in most of the samples show that the chromitites in Cuobuzha are typical of high-Cr varieties, with Cr numbers [$Cr^\# = 100 \times Cr/(Cr + Al)$] ranging from 75 to 78, and Mg numbers [$Mg^\# = 100 \times Mg/(Mg + Fe^{2+})$] ranging from 66 to 69 (Zhao et al., 2019).

4 Analytical Methods

Petrographic examinations of 60 thin sections from 18 samples provided detailed textural and mineralogical data. Microprobe analyses of minerals in selected samples were carried out on polished thin sections using a JEOL JXA-8100 electron-probe micro-analyzer (EPMA) at the State
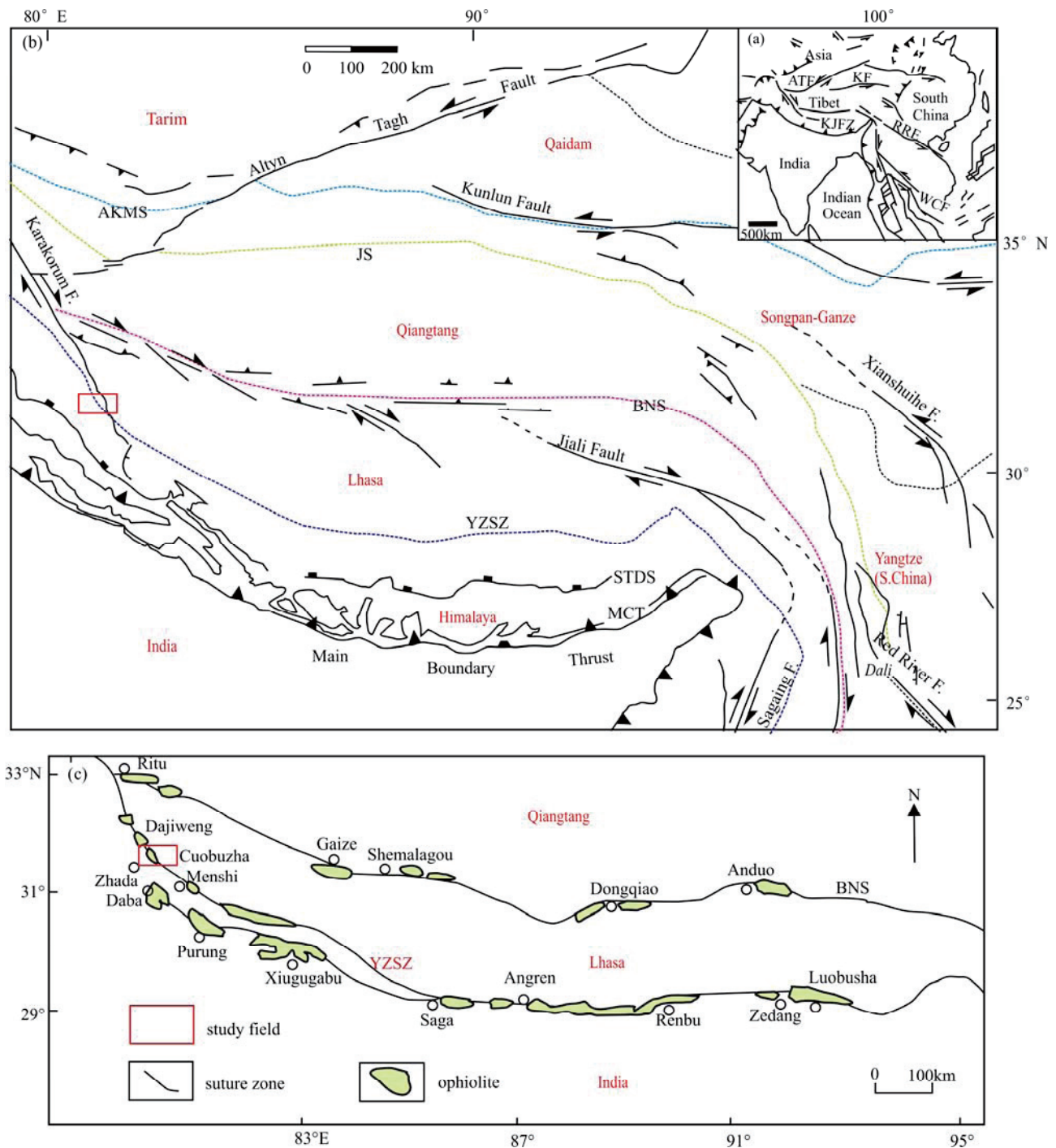
Fig. 1. Tectonic sketch map of Tibet (modified from Yin et al., 2003 and Liu et al., 2015).
(a) Index map showing the location of the Tibet Plateau in Asia; (b) Simplified geological map of the Tibetan plateau and surrounding areas; (c) Distribution of the ophiolites along the YZSZ and BNS in southern Tibet.
Key for abbreviations: MBT, Main Boundary Thrust; MCT, Main Central Thrust; STDS-South Tibet Detachment System; YZSZ, Yarlung Zangbo Suture Zone; BNS, Bangong – Nujiang Suture; JS, Jinsha Suture; AKMS, Ayimaqin – Kunlun – Muztagh Suture; ATF, Altyn Tagh Fault; KF, Kunlun Fault; KJFZ, Karakorum – Jiali Fault Zone; RR, Red River Fault; WCF, Wang Chao Fault; GCT, Great Counter Thrust; ZGT, Zhongba – Gyangze Thrust.

Key Laboratory Breeding Base of Nuclear Resources and Environment, Nanchang, China. This instrument is equipped with 3 wavelength-dispersive spectrometers and an energy-dispersive Oxford INCA spectrometer. Analytical conditions were set at a 15 kV accelerating voltage, and a 20 nA beam current with a 2 μm beam diameter. Well-characterized natural minerals and synthetic oxide standards were used for calibration. Raw data were reduced with an EPMA online correction procedure, including background, dead time and a ZAF-correction program. Accuracy and precision were checked against SPI standards and were within ~2 wt % limits
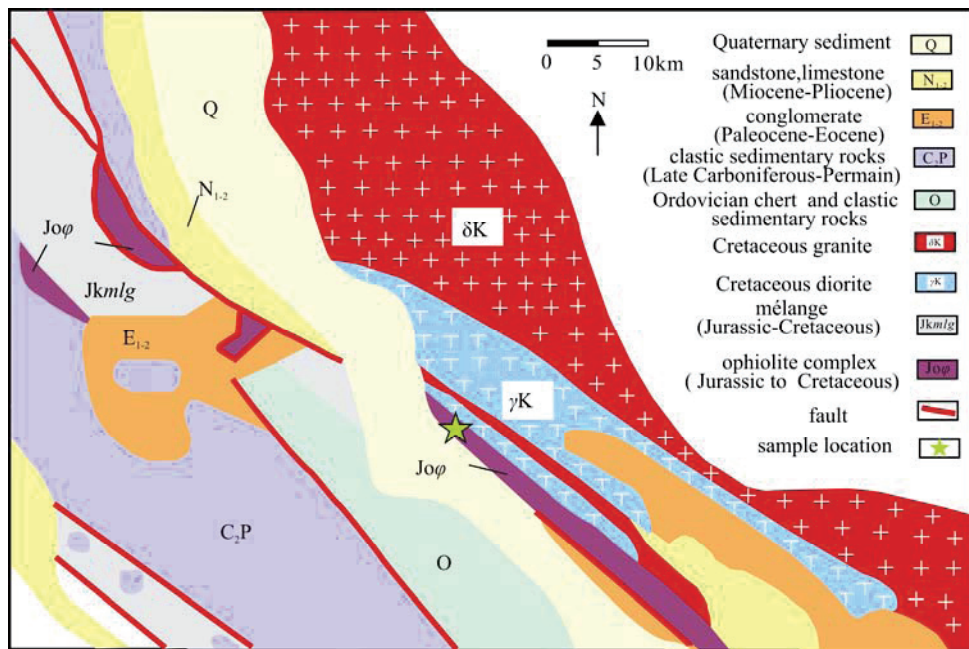
Fig. 2. Detailed geological map of the Cuobuzha area in southern Tibet modified from Feng et al., 2015.
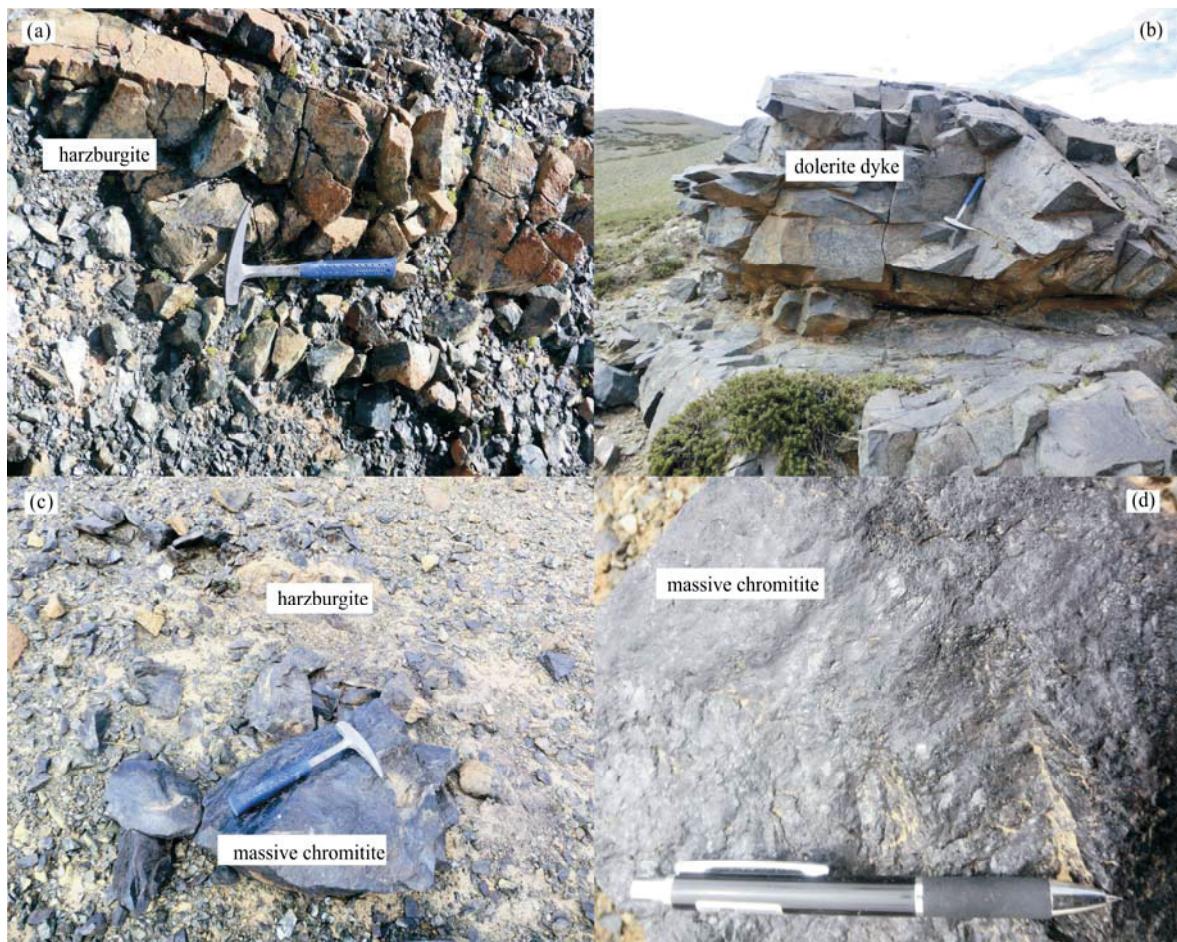

Fig. 3. Field occurrences of the Cuobuzha ophiolite.

relative to the major elements.

In situ trace element analyses were conducted by Laser Ablation Inductively Coupled Plasma Mass Spectrometer (LA-ICP-MS) at the State Key Laboratory of Ore Deposit Geochemistry, Institute of Geochemistry Chinese Academy of Sciences (IGCAS). Laser sampling was

performed using a 193 nm ArF excimer laser (GeoLas Pro). An Agilent 7700x Inductively Coupled Plasma Mass Spectrometer (ICP-MS) instrument was used to acquire ion-signal intensities. Helium (580 ml/min) was applied as a carrier gas. Argon (900 ml/min) was used as the make-up gas and mixed with the carrier gas via a Y-connector before entering the ICP. Each analysis incorporated a background acquisition of approximately 30 s (gas blank) followed by 60 s of data acquisition from the sample. Analyses were run with 44 μm pit size, 5 Hz pulse frequency and 9 J cm^{-2} fluence. We used ^{57}Fe as the internal standard and the values were acquired by EPMA. Two standards, a komatiite glass (GOR-128), and natural chrome (QC-Cr) was analyzed as unknown samples to monitor the data quality. The preferred values of element concentrations for the United States Geological Survey (USGS) reference glasses are from the GeoReM database (http://georem.mpch-mainz.gwdg.de/).

We selected 18 fresh chromitites for whole-rock geochemical analysis at the China National Research Center of Geoanalysis. Major elements were determined by X-ray fluorescence on fused glass beads using PW4400 spectrometry. The analytical precision is better than 5%. The PGE abundances of the chromitites were obtained by a combined NiS fire assay and ICP-MS method (Sun et al., 1993; Zhou et al., 1998). Preconcentration of the PGEs was achieved by NiS fire assay followed by Te coprecipitation of the PGEs. The fire assay mixture was prepared using powdered chromitite (10 g), nickel oxide (2 g), sulfur (1.25 g), sodium carbonate (15 g), sodium borate (20 g), silica (1g) and flour (1 g) to produce a NiS button. Then the mixture was put into clay crucible and fused in an assay furnace at 1200 °C for 1.5 h. Crushed buttons were dissolved in 100 mLs of concentrated HCl, and the PGEs were collected by Te coprecipitation. Solutions were analyzed for PGEs using a TJAPQEXCELL ICP-MS. Total procedural blanks are 0.3 ng for Os, Ru, Rh, Ir , and 0.06 ng for Pt, and Pd. Average determined abundances of Ru, Rh, Pd, and Ir were found to be within error of the certified values of the rock standards.

5 Results

5.1 In situ trace element chemistry

The average Ga, Ni, Zn, Co, Mn, V, and Sc concentrations of chromites in the Cuobuzha chromitites are 18, 1360, 298, 178, 1628, 506, and 4 ppm, respectively (Table 1). Accessory chromites in the harzburgites have higher average concentrations of Ga (44 ppm), Zn (1750 ppm), Co (370 ppm) and V (640 ppm), and lower average concentrations of Mn (964 ppm) and Sc (0.8 ppm). The compositions of chromites are plotted normalized to the compositions of chromites from MORB (Fig. 5a). From the figure, it is evident that chromites of the Cuobuzha chromitites are depleted in Al, Ga, Zn, V and Mg, and enriched in Cr and Mn, showing a very similar profile to those of Bonin (BON) and Thetford Mines Ophiolite (TMO) boninites. However, there are some differences: chromites in the Cuobuzha chromitites are strongly enriched in Ti and Ni, and depleted in V, Fe, and Zn compared to the boninites. Accessory chromites in the harzburgites are relatively depleted in Ti and Sc, and enriched in Co and Zn, displaying a completely different profile from those observed in the chromitites (Fig. 5b).

5.2 Whole rock PGE chemistry

Platinum group elements (PGEs) occur abundantly in the Cuobuzha chromitites; their concentrations are as follows: Os 150–352 ppb, Ir 88.1–185 ppb, Ru 81.9–143 ppb, Rh 6.39–10.5 ppb, Pt 1.31–8.38 ppb, and Pd 0.4–4.56 ppb (Table 2). Collectively, the chromitites are characterized by low Pd/Ir ratios (<0.1), are enriched in Os and Ir, and depleted in Rh, Pt and Pd as observed from the primitive mantle normalized diagram (Fig. 6). All samples show significantly negative Ru anomalies. With the exception of three samples, others display negative slope from Pt to Pd. The whole-rock total PGE abundance of the harzburgites (ΣPGE = 22.31–36.12 ppb) is lower than that of the chromitites (ΣPGE = 380–577 ppb) (Feng et al., 2016). In the mantle normalized plot, the harzburgites have relatively flat patterns with higher Pd/Ir ratios (0.54–1.89) (Fig. 6). The Os, Ir, and Ru concentrations of the chromitites are much higher than those of the harzburgites, whereas the Rh, Pt, and Pd concentrations are lower.

5.3 Inclusions within chromites
5.3.1 Platinum group mineral (PGM) inclusions

Approximately twenty PGM grains were discovered in the chromitite samples; these are shown in Fig. 7. Most of them are Ru, Os, and Ir minerals, including alloys,

Table 1 Trace elements compositions of chromites from the Cuobuzha ophiolite (concentrations in ppm) by LA-ICP-MS analysis

	Sample	Ga	Ti	Ni	Zn	Co	Mn	V	Sc
chromitite	14kc-10-1	18.62	1020.00	1377.93	277.84	177.24	1650.00	495.92	4.90
	14kc-10-2	18.36	858.00	1461.09	277.14	174.07	1502.82	507.30	4.75
	14kc-10-3	19.24	1848.00	1499.18	308.20	176.73	1572.54	540.10	5.28
	13YL-30-26-2	18.69	1428.00	1603.58	316.60	176.14	1533.80	535.53	5.26
	13YL-30-26-3	18.06	1386.00	1515.35	304.64	174.04	1440.85	523.72	5.17
	13YL-30-26-4	17.29	1428.00	1561.51	302.87	177.77	1471.83	518.98	4.79
	13YL-30-27-6	18.23	1680.00	1072.07	315.59	190.14	1650.00	486.30	1.75
	13YL-30-27-7	17.55	1680.00	1071.99	304.07	182.54	1990.85	478.72	2.19
	13YL-30-27-8	16.95	1386.00	1080.12	278.60	176.78	1835.92	463.79	1.62
harzburgite	13YL-30-15-1	48.36	202.18	1895.03	1864.25	433.52	998.62	674.39	0.75
	13YL-30-15-2	36.96	163.80	1512.94	1513.04	326.67	859.66	549.16	0.98
	13YL-30-15-3	50.32	213.25	1958.46	1973.16	433.35	988.28	718.01	1.02
	13YL-30-15-4	37.97	168.27	1410.03	1449.78	337.48	810.77	539.35	0.42
	13YL-30-12-1	48.67	483.93	1479.72	2014.51	359.09	1111.01	695.84	0.78
	13YL-30-12-2	40.08	520.99	1230.43	1688.39	328.78	1015.36	663.47	0.59

Table 2 PGE concentrations of the Cuobuzha chromitite (concentrations in ppb)

| Sample	Os	Ir	Ru	Rh	Pt	Pd	Total	Pd/Ir
14KC-1	154	104	104	8.49	5.83	4.56	380.88	0.044
14KC-2	183	128	104	8.51	5.18	3.9	432.59	0.030
14KC-3	205	128	81.9	7.24	2.37	0.93	425.44	0.007
14KC-4	151	88.1	91.2	6.39	1.31	0.38	338.38	0.004
14KC-5	246	147	105	8.33	2.61	0.68	509.62	0.005
14KC-6	219	150	123	9.22	3.08	0.73	505.03	0.005
14KC-7	186	173	112	9.76	2.93	0.9	484.59	0.005
14KC-8	212	150	124	9.4	2.61	0.57	498.58	0.004
14KC-9	207	122	101	8.48	2.67	0.38	441.53	0.003
14KC-10	352	124	89.8	8.61	2.07	0.67	577.15	0.005
14KC-11	222	185	105	9.09	3.83	0.47	525.39	0.003
14KC-12	150	120	111	8.32	1.94	0.9	392.16	0.008
14KC-13	208	142	97	7.98	2.27	0.49	457.74	0.003
14KC-14	124	113	109	9.22	5.98	3.82	365.02	0.034
14KC-15	218	180	125	10.5	3.3	0.51	537.31	0.003
14KC-16	236	176	110	11	8.38	6.1	547.48	0.035
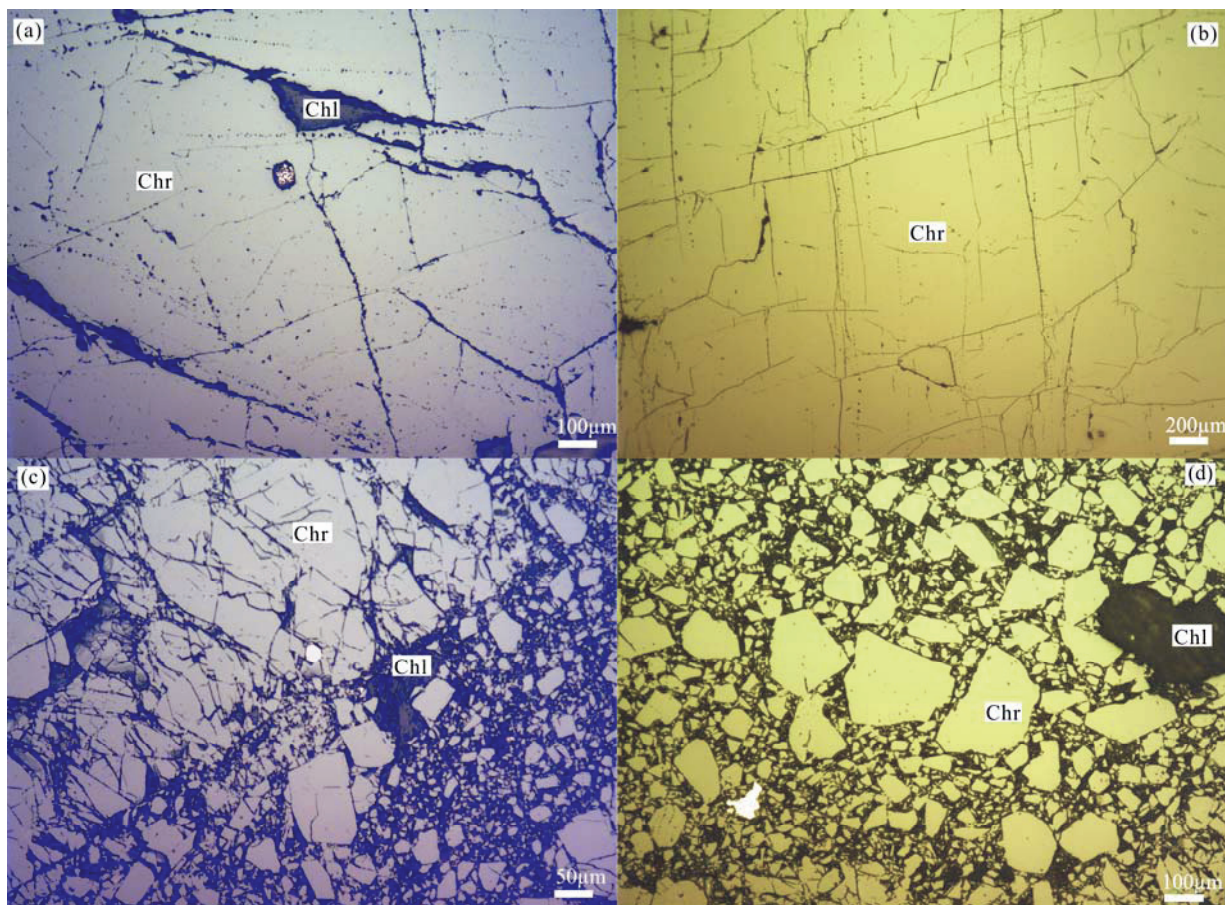
Fig. 4. Photomicrographs of the Cuobuzha chromitites (Chr: chromite; Chl: chlorite).

sulfides, and sulfarsenides. They occur within unaltered chromite grains as subhedral-euhedral inclusions, less than 20 μm across. Ruthenium is mainly present as laurite. Osmium is present as erlichmanite and Os-Fe alloy, and substitutes for Ru in laurite. Iridium is present in both Ru and Os minerals, and forms sulfides (e.g., cuproiridsite) and sulfarsenides (e.g., irarsite). Os, Ir, and Ru contents of laurite are 23.06 wt%, 4.86 wt% and 34.89 wt%, respectively (Table 3). Two erlichmanite grains contain Os (41.77–42.24 wt%), Ir (6.61–12.21 wt%), and Ru (14.80– 15.75 wt%). The Os-Fe alloys form polygonal crystals, in

which Os and Fe contents range from 31.39–46.86 wt % and 7.34–32.63 wt%, respectively. Variable amounts of Ni (2.38 – 19.66 wt %), Ru (2.92 – 17.57 wt%), and Ir (5.93 – 9.33 wt%) are also detected in these Os-Fe alloys. One cuproiridsite grain occurs as a solitary inclusion up to 10 μm in size, which mainly contains Ir (53.81 wt%) and Cu (11.42 wt%) with minor contents of Pt (2.51 wt%) and Rh (3.95 wt %). One irarsite grain occurs along the rim of millerite, forming a muti-phase inclusion, which contains Ir (48.93 – 49.64 wt %), S (12.16–12.93 wt %), and As (32.4–33.3 wt %).
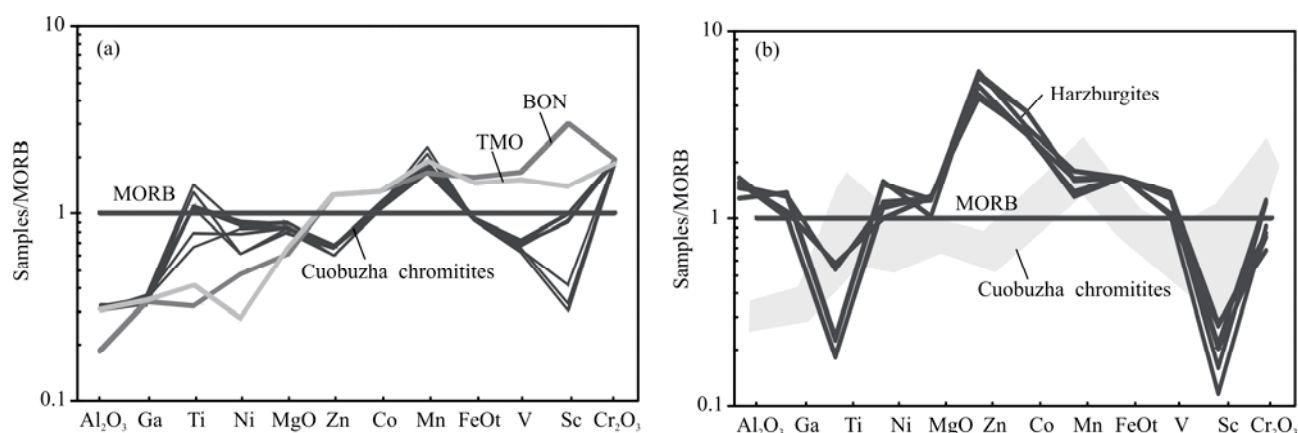
Fig. 5. MORB-normalized trace element diagrams of chromites in Cuobuzha.
(a) MORB-normalized trace element diagrams of chromites from the Cuobuzha chromitites; (b) MORB-normalized trace element diagrams of chromites from the Cuobuzha harzburgites. Data for chromites of the Bonin Island boninite (BNO), the Thetford Mines Ophiolite crust (TMO) and MORB are from Pagé et al., 2009.
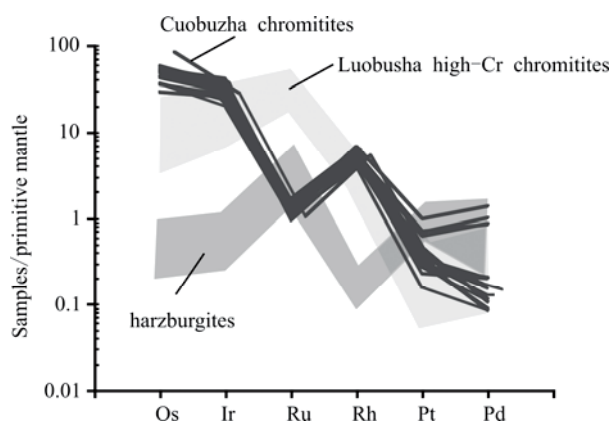

Fig. 6. Primitive mantle-normalized PGE patterns for the chromitites and harzburgites from the Cuobuzha ophiolite as well as the high-Cr chromitites from the Luobusha ophiolite.
The values for the Cuobuzha harzburgites and the Luobuzha chromitites are from Feng et al., 2016 and Zhou et al., 1996, respectively. Normalized values are from Barnes et al., 1988.

5.3.2 Fe-Ni and Fe-Cr alloy

In the Cuobuzha chromitites, two kinds of Fe-Ni alloys are identified: primary and secondary. Primary Fe-Ni alloys occur as inclusions in chromite or clinopyroxene grains (Fig. 8a, b). They are subhedral to euhedral and range from 10 to 20 μm. Their main component is Ni ($Cr_{0-3}Fe_{23-27}Ni_{67-73}$, Table 3). Secondary Fe-Ni alloys are common as tiny grains in serpentine or as relatively larger fracture fillings (Fig. 8c). One Fe-Cr alloy, which is euhedral and less than 5 μm across, is present as an inclusion within a chromite grain. Its main constituent is Fe ($Cr_{13}Fe_{87}$).

6 Discussion

6.1 Parental magma compositions

The chemistry of chromites strongly depends on the compositions of their parental magmas (Dick and Bullen, 1984; Kamenetsky et al., 2001; Pagé and Barnes, 2009).

Based on this relationship between them, the compositions of melts from which chromites are crystallized at equilibrium can be determined (Maurel et al., 1982, 1984; Kamenetsky et al., 2001; Rollinson et al., 2008). Zhao et al. (2019) calculated the Al_2O_3, and TiO_2 contents, and FeO/MgO ratios of the parental melts. Their results showed that the Al_2O_3 and TiO_2 contents of the melts were 11.27–12.1 wt% and 0.19–0.4 wt%, respectively, while calculated FeO/MgO ratios were in the range of 0.51–0.65 (Zhao et al., 2019). Comparisons of the compositions between the calculated parental melts and the primitive magmas from different tectonic settings indicate that the melts in equilibrium with the Cuobuzha chromitites have boninite hallmarks (Fig. 9).

Experimental studies show that V, Zn, and Co are compatible (D ~ 3.8–10.2), Ga and Ni are moderately compatible (D ~ 1.3–3.3), while Mn, Ti, and Sc are slightly to moderately incompatible (D ~ 0.2–1.1) with chromites (Pagé and Barnes, 2009). Based on these partition coefficient values (D), a rough estimation of the trace element compositions of the parental melts was made. Calculated results reveal the following composition of the parental melts: Ga, 9–11 ppm; Ti, 1144–2240 ppm; Ni, 948–1419 ppm; Zn, 40–46 ppm; Co, 45–48 ppm; Mn, 1470–2031 ppm; V, 60–69 ppm; and Sc, 8–26 ppm. In the MORB-normalized plot, except Ni and Zn, the parental melts exhibit similar patterns to that of boninites (Fig. 10).

In general, podiform chromitites have variable PGE concentrations, usually less than 500 ppb, as well as very low Pd_N/Ir_N ratios (<0.1) (Leblanc, 1992; Tian et al., 2019; Zhou et al., 1998, 2014). In addition, high-Cr chromitites have higher PGE contents than high-Al chromitites (Zhou et al., 1998). The PGEs are sensitive to the degrees of partial melting in source regions and the S-saturation status of the parental magmas (Hamlyn et al., 1985; Sun et al., 1991; Keays, 1995; Zhou et al., 1998, 2014). Low degree partial melting of primitive mantle produces S-saturated melts, leaving behind sulfides in the residual peridotites (Hamlyn et al., 1985; Zhou et al., 1998). Subsequent re-melting of these depleted peridotites generates strongly S-undersaturated magmas, because

Table 3 Electron microprobe results (concentrations in wt%) of the inclusions hosted in chromites of the Cuobuzha chromitite

	Sample	Os	Ir	Ru	Rh	Pt	Pd	Ni	Fe	Cu	Cr	S	As	Sb	Total
Fe-Ni alloy	14KC-7.3	0.05	0.00	0.02	0.09	1.77	0.06	67.97	26.57	0.12	2.48	0.08	0.00	0.01	100.47
	14KC-7.4	0.00	0.00	0.00	0.01	0.00	0.00	69.15	24.81	0.20	1.34	0.38	0.00	0.00	96.71
	14KC-7.5	0.00	0.00	0.08	0.03	0.00	0.00	67.30	25.66	0.21	3.85	0.01	0.00	0.00	98.60
	14KC-2.3	0.30	0.00	0.00	0.00	1.24	0.03	65.55	24.66	0.41	2.74	0.29	0.06	0.08	96.22
	14KC-5.2	0.47	0.44	0.00	0.00	0.00	0.00	70.31	25.50	0.26	2.37	0.30	0.00	0.09	100.40
	14KC-9.4	0.00	0.26	0.00	0.06	0.54	0.00	70.74	25.87	0.34	2.21	0.03	0.00	0.00	100.50
	14KC-9.5	0.08	0.03	0.02	0.00	0.00	0.07	70.14	25.68	0.10	1.73	0.06	0.00	0.00	98.46
	14KC-9.9	0.00	0.00	0.00	0.11	0.00	0.01	70.57	25.29	0.06	2.13	0.01	0.00	0.05	98.74
	14KC-9.10	0.00	0.26	0.00	0.00	0.00	0.00	70.73	25.55	0.24	1.85	0.01	0.07	0.00	99.19
	14KC-4.1	0.00	0.00	0.00	0.00	0.00	0.00	67.81	25.17	0.32	3.12	0.06	0.13	0.00	97.14
	14KC-4.3	0.00	0.27	0.00	0.04	1.24	0.00	69.01	25.74	0.34	2.88	0.04	0.01	0.00	100.21
	14KC-4.4	0.00	0.00	0.02	0.01	2.04	0.00	68.93	26.73	0.24	1.51	0.02	0.00	0.00	100.13
	14KC-4.5	0.00	0.00	0.00	0.02	0.11	0.00	69.67	26.52	0.34	0.67	0.02	0.17	0.05	98.17
	14KC-4.7	0.08	0.00	0.02	0.06	0.00	0.00	70.62	25.32	0.27	2.39	0.00	0.25	0.00	99.78
	14KC-8.2	0.06	0.00	0.00	0.00	0.97	0.03	70.55	25.44	0.07	0.44	0.66	0.14	0.00	99.65
	14KC-8.4	0.00	0.04	0.00	0.01	0.00	0.05	73.18	25.60	0.27	0.92	0.35	0.00	0.09	101.41
	14KC-8.5	0.23	0.00	0.06	0.00	0.00	0.00	69.19	25.21	0.26	1.08	0.66	0.18	0.00	98.74
	14KC-8.8	0.00	0.00	0.02	0.00	0.76	0.00	68.98	25.58	0.35	0.61	0.34	0.09	0.00	97.64
	14KC-8.9	0.92	0.00	0.02	0.00	0.97	0.01	66.35	28.24	0.17	0.43	0.55	0.22	0.00	101.10
	13YL-32.3	0.00	0.00	0.04	0.00	0.65	0.05	71.77	25.61	0.40	0.31	0.13	0.12	0.04	99.98
	13YL-32.8	0.23	0.18	0.08	0.00	1.08	0.03	68.23	25.55	0.70	0.60	0.03	0.00	0.00	97.61
	13YL30-20.1	0.00	0.07	0.00	0.02	0.00	0.05	68.81	25.79	0.45	0.95	0.06	0.12	0.00	97.28
	13YL30-20.2	0.00	0.43	0.00	0.04	0.59	0.00	69.04	24.05	0.10	1.25	0.15	0.13	0.00	96.75
	13YL30-24.1	0.00	0.47	0.00	0.04	1.08	0.00	70.99	26.00	0.24	0.12	0.17	0.14	0.01	99.37
	13YL30-24.2	0.08	0.15	0.01	0.02	0.00	0.11	71.14	25.32	0.18	0.40	0.11	0.13	0.00	98.39
	13YL30-24.3	0.15	0.00	0.00	0.02	0.00	0.00	71.21	26.35	0.25	0.37	0.10	0.00	0.17	99.18
	13YL30-24.4	0.80	0.00	0.02	0.00	0.00	0.00	69.53	25.97	0.30	1.35	0.07	0.00	0.00	98.55
	13YL30-23.1	0.33	0.53	0.00	0.00	0.11	0.04	70.96	26.35	0.30	0.41	0.07	0.17	0.00	99.95
	14KC-13.1	0.67	0.00	0.00	0.02	0.11	0.07	68.27	25.09	0.27	1.81	0.23	0.00	0.09	97.12
	13YL-30-21.2	0.98	0.88	0.00	0.07	0.37	0.00	70.53	25.79	0.48	0.41	0.03	0.05	0.00	100.19
Os-Ru-Ir-Fe-Ni	13YL-32.6	46.86	8.73	3.29	0.03	0.00	0.09	2.38	28.81	0.08	0.65	0.67	0.18	0.00	98.87
	13YL-32.7	45.59	8.97	2.92	0.10	0.00	0.00	2.53	32.63	0.00	0.64	0.93	0.09	0.00	101.28
	13YL30-23.2	37.67	5.93	13.71	0.33	0.00	0.27	19.66	18.58	0.10	3.06	0.06	0.00	0.00	100.05
RuS$_2$	14KC-13.2	23.06	4.86	34.89	0.30	0.00	0.62	0.03	0.56	0.00	1.30	34.54	0.00	0.01	100.17
OsS$_2$	14KC-5.5	42.24	12.21	14.80	0.21	0.00	0.36	0.13	1.05	1.09	1.36	28.19	0.00	0.10	96.57
	14KC-1.6	41.77	6.61	15.75	0.79	0.00	0.32	0.83	0.94	0.00	1.59	27.77	0.00	0.16	96.53
CuIr$_2$S$_4$	14KC-7.1	0.00	53.81	0.12	3.95	2.51	0.00	1.70	0.60	11.42	1.73	23.35	0.00	0.00	99.18
IrAsS	14KC-6-1	0.69	49.64	0.52	1.43	0.00	0.15	0.96	0.65	0.03	2.34	12.93	32.40	0.11	101.88
	14KC-6-3	0.95	48.93	0.31	1.00	1.34	0.00	0.35	0.71	0.01	2.73	12.16	33.30	0.14	101.92
Ni$_3$S$_2$	14KC-1.1	0.27	0.00	0.00	0.03	0.22	0.00	67.74	0.85	0.31	1.99	26.76	0.07	0.02	98.26
	14KC-1.2	0.00	0.08	0.00	0.04	0.00	0.00	67.14	0.92	0.26	2.39	26.27	0.00	0.00	97.12
	14KC-1.4	0.00	0.00	0.00	0.00	1.18	0.00	67.38	1.21	0.04	2.75	26.81	0.02	0.08	99.56
	14KC-1.5	0.00	0.00	0.00	0.00	0.00	0.10	67.36	0.91	0.07	2.73	26.22	0.21	0.00	97.62
	14KC-1.7	0.00	0.42	0.00	0.00	0.56	0.00	68.01	0.63	0.01	1.83	26.42	0.00	0.00	97.87
	14KC-1.8	0.51	0.00	0.00	0.00	0.34	0.07	65.58	0.92	0.03	2.32	28.30	0.05	0.00	98.15
	14KC-14.1	0.00	0.37	0.00	0.09	0.22	0.01	67.20	0.89	0.00	3.06	27.18	0.00	0.00	99.07
	14KC-14.2	0.00	0.42	0.00	0.09	0.39	0.01	66.45	0.86	0.01	2.86	26.14	0.25	0.01	97.53
	14KC-14.3	0.27	0.39	0.00	0.02	0.00	0.00	66.84	0.30	0.03	0.89	28.90	0.00	0.00	97.66
NiS	14KC-6-2	0.00	3.30	0.08	0.41	0.00	0.08	56.51	0.87	0.29	2.64	31.53	4.44	0.00	100.21
Fe-Cr	14KC-4-6	0.00	1.08	0.00	0.02	0.00	0.02	0.12	85.68	0.16	12.60	0.04	0.07	0.00	99.99

majority of sulfur in the primitive mantle has already been removed during extraction of melts at the first stage. Therefore, S-undersaturated magmas are rich in PGEs (Zhou et al., 1998). Accordingly, based on their high PGE concentrations, we infer that the parental magmas of the Cuobuzha chromitites are S-undersaturated.

6.2 Crystallization conditions of the Cuobuzha chromitite
6.2.1 Implications from PGM inclusions

Two major hypotheses have been proposed to explain the occurrence of PGM inclusions in chromites: i) the PGM inclusions are exsolved from the chromite host at a subsolidus stage (Gijbels et al., 1974; Naldrett and Cabri, 1976; Ferrario and Garuti, 1990), or ii) they are magmatic minerals that are precipitated at an early stage, followed by their mechanical encapsualtion into the growth surfaces of chromite crystals (Augé, 1988; Constantinides et al., 1980; Stockman and Hlava, 1984).

Exsolution of PGM from chromites has been definitely undermined by the "metal clusters" hypothesis (Tredoux et al., 1995), which does not require any crystal-chemical compatibility of individual PGE in favor of the spinel structure. This theory states that clusters, which are composed of a few hundred atoms of PGE, initially suspend in the melt at a high temperature. Due to their physical and chemical properties, the clusters coalesce to form PGM alloys or sulfides and are subsequently enclosed into early-crystallizing chromites and silicates. The cluster model provides an explanation of the
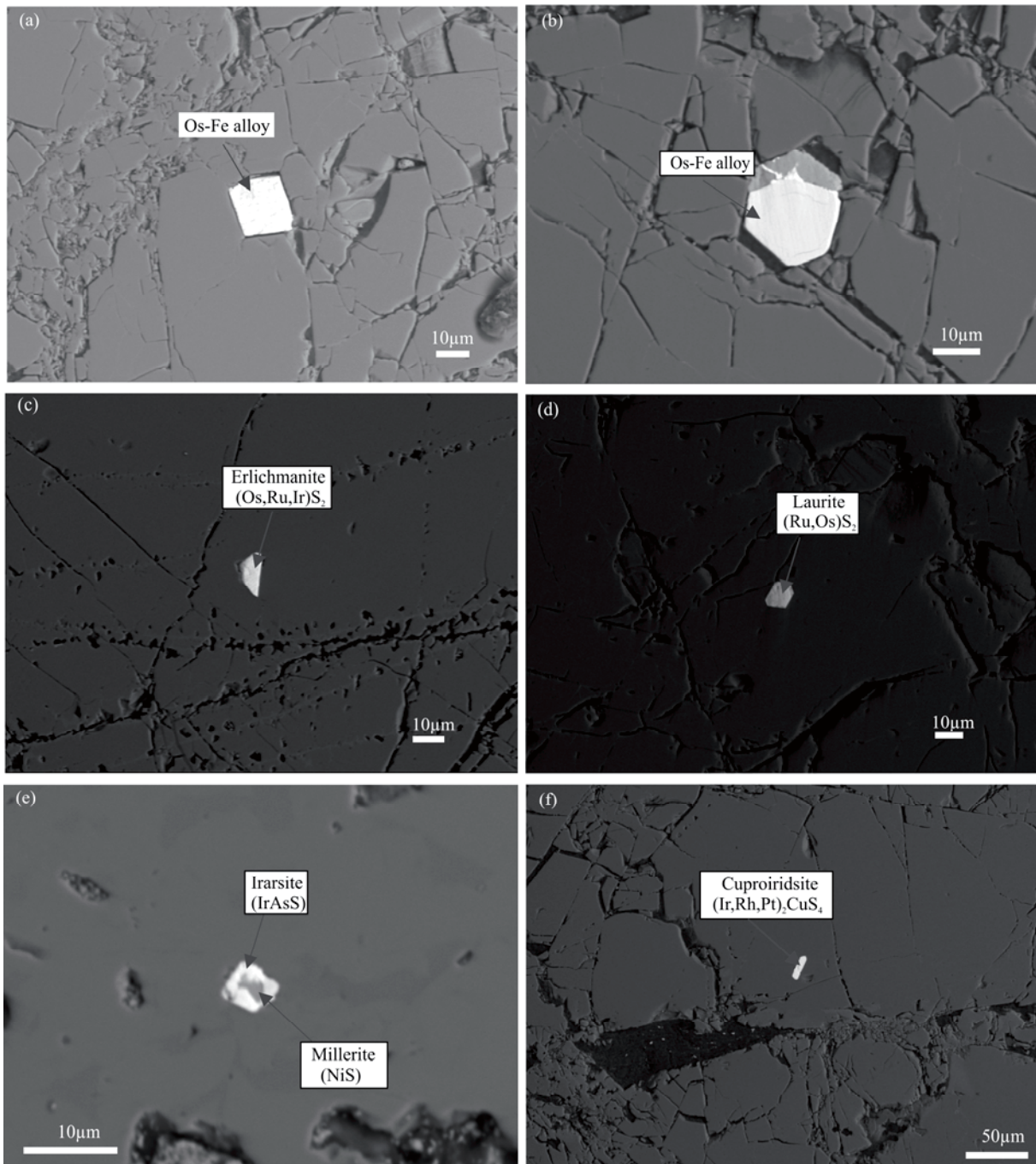
Fig. 7. The Backscatter Electron (BSE) images of PGMs inclusions hosted in the chromite grains.

similarity of PGM species between coexisting chromite and forsterite, which is a feature that strongly argues against PGM exsolution from chromites (Gijbels et al., 1974; Naldrett and Cabri, 1976; Ferrario and Garuti, 1990). Based on LA-ICP-MS, Later works confirmed the existence of these sub-micron PGE-bearing alloys (Ballhaus and Sylvester, 2000; Sattari et al., 2002; Locmelis et al., 2011; Pagé et al., 2012).

The paragenesis and compositions of PGMs have been used to estimate specific thermodynamic conditions, such as sulfur fugacity and temperature prevailing in the magmatic system, before and during the crystallization of

chromites (Augé, 1988; Nakagawa and Franco, 1997; Garuti et al., 1999). Experimental results indicate that nearly pure laurites (RuS_2) are crystallized from the melts under high temperature (1200–1300°C) and low sulfur fugacity [log $f(S_2)$ = −2 to −1] (Brenan and Andrews, 2001; Bockrath et al., 2004)]. When temperature decreases, $f(S_2)$ gradually increases and Ru in laurites may be partly replaced by Os, finally leading to the formation of Os-rich laurites (Garuti et al., 1999). Therefore, PGMs are generally crystallized in the order of Os-Ir-Ru alloys, Ru-rich laurites, and Os-rich laurites (Stockman and Hlava, 1984; Brenan and Andrews, 2001;
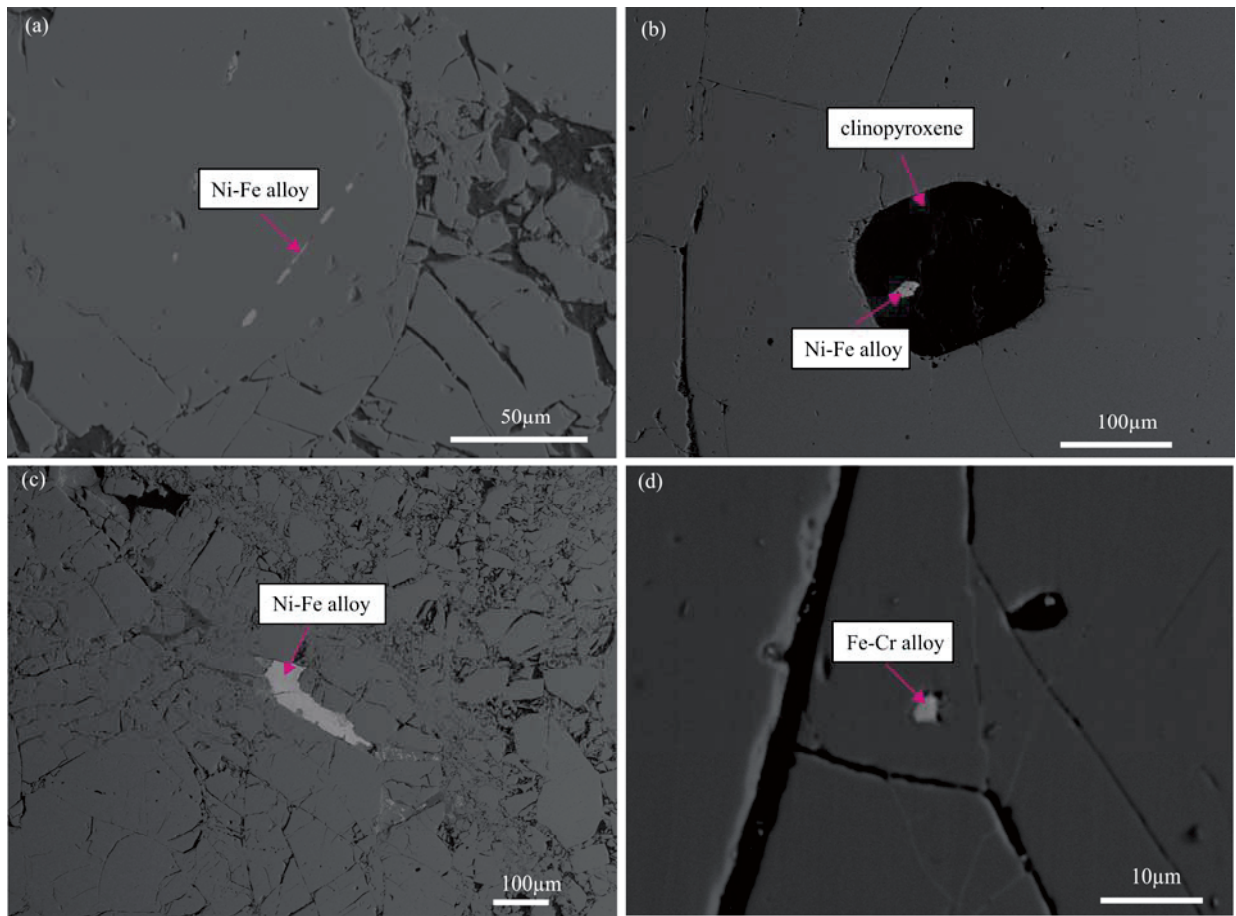
Fig. 8. The Backscatter Electron (BSE) images of PGMs inclusions hosted in the chromite grains.
(a) Several primary Fe-Ni alloys arrange in linear trails within a single chromite grain; (b) One polygonal primary Fe-Ni alloy occurs within a single clinopyroxene grain; (c) One secondary Fe-Ni is anhedral and occurs as interstitial crystals between chromite grains; (d) One euhedral primary Fe-Cr alloy occurs in a single chromite grain.
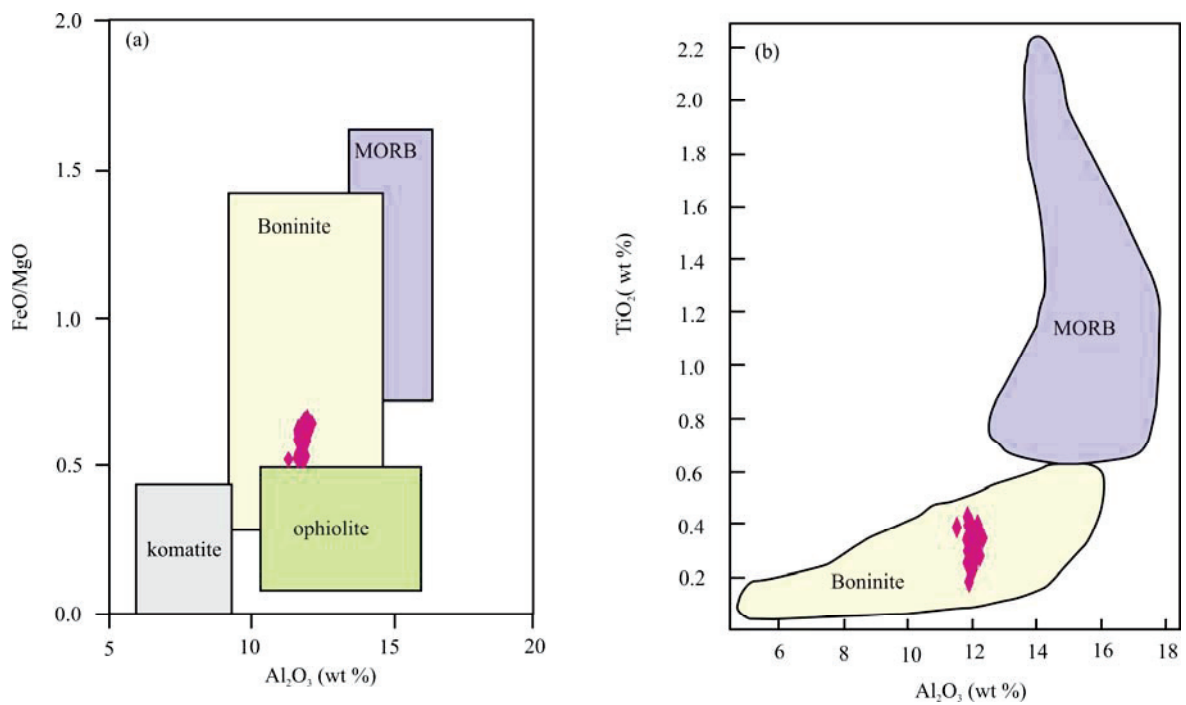

Fig. 9. Plots of the estimated compositions of the parental magmas.
(a) Plot of Al_2O_3 contents and FeO/MgO values of the parental magmas (Barnes and Roder., 2001); (b) Plot of Al_2O_3 and TiO_2 contents of the parental magmas (Pagé and Barnes., 2009).
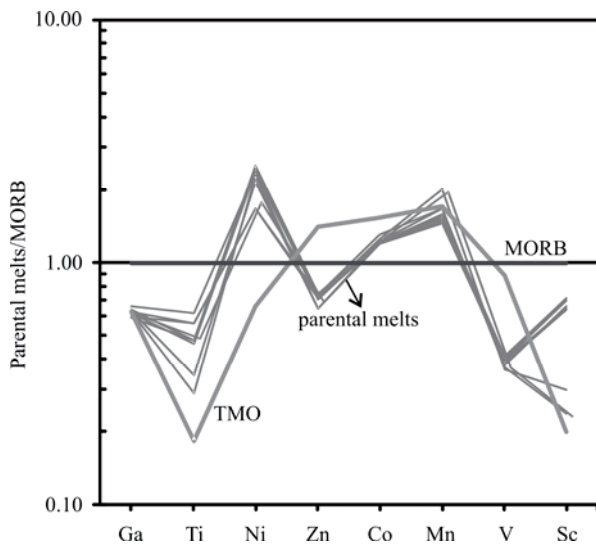
Fig. 10. MORB-normalized trace element diagram of the parental magmas.
Data for chromites of the BNO, TMO and MORB are from Pagé et al., 2009.
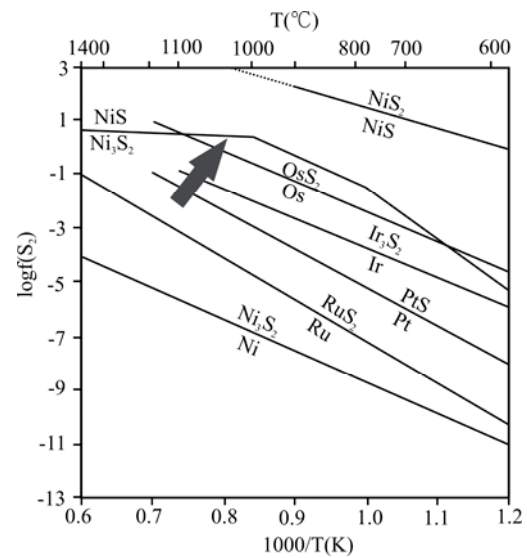

Fig. 11. Metal-sulphide equilibrium curves (Melcher et al., 1997; Garuti et al., 1999).
The red arrow indicates the proposed crystallization trend of T-f(S2) for the Cuobuzha chromitite (see text for detailed discussion).

Bockrath et al., 2004; Distler et al., 2008).

The PGM assemblages in the Cuobuzha chromitites indicate that $f(S_2)$ was initially low enough to allow precipitation of Os-Fe alloys, which was followed by the crystallization of laurites from Ru-(Os) -S precursors (Fig. 11). Substitution of Os for Ru in laurites increased with decreasing temperature (T). When $f(S_2)$ is high enough, cuproiridsites became stable. The presence of sulfarsenides (Fig. 7e) as primary inclusions proved an appreciable activity of As in the system at high temperature. In addition, the fact that irarsites occur along the rim of millerite (Fig. 7e) suggests later crystallization of irarsites than millerites.

6.2.2 Implications from the Fe-Ni and Fe-Cr alloys

Secondary Fe-Ni alloys are interpreted as the reaction products of Fe-Ni sulfides under oxidizing conditions (Bai et al., 2004), implying that they could not indicate the crystallizing conditions for the chromitites. Thus, in the following text, we just discuss the primary Fe-Ni and Fe-Cr alloys.

A considerable number of studies have shown that oxygen fugacity (fO_2) is close to the fayalite-magnetite-quartz buffer ($\Delta\log fO_2$ [FMQ] $\approx \pm 2$) at the top of the upper mantle (< 60 km) due to the concentration of Fe^{3+} in modally minor phases, but with increasing depth, it decreases to the iron-wustite buffer (IW, $\Delta\log fO_2$ [FMQ] ≈ -5) at ≥250 km (Frost et al., 2004, 2008). At the 410 km discontinuity, redox condition lies below the iron-wüstite buffer (Woodland and Koch, 2003). Fe-Ni alloys are mainly found in meteorites and rarely occur in terrestrial rocks. Experimental modeling indicates that Ni-rich Fe metals become stable when oxygen fugacity value is close to the iron-wustite buffer at approximately 8 GPa. The formation of Ni-Fe metals results from the disproportionation of FeO to produce metals and Fe_2O_3-bearing garnets, which is demonstrated by high $Fe^{3+}/\Sigma Fe$

ratios in minerals in equilibrium with metallic Fe (Frost et al., 2004; Lauterbach et al., 2000). Available experiments imply that Fe-rich metals can be stable throughout the transition zone, and an order of 1 wt% metallic Fe would be forced to precipitate if the lower mantle has a typical bulk silicate earth (BSE) composition (Frost et al., 2004, 2008). Golubkova et al. (2016) calculated the phase relations for a model peridotite composition with 0.1 wt% carbon. Their results show that at upper mantle conditions, chromites are reduced to Fe-Cr alloy at fO_2 values ranging between 2.2 – 3.8 log units below the iron-wustite buffer. Thus, primary Ni-rich Fe-Ni and Fe-Cr alloys in the Cuobuzha chromitites are typical highly reduced phases and are formed below the IW buffer (≥250km).

6.3 Origin of the Cuobuzha chromitites

The mainstream understanding for podiform chromitites is that they are formed through melt/rock reaction between tholeiitic or boninitic melts and peridotites, which is evidenced by the commonly occurring hydrous mineral inclusions in most chromitites (Zhou et al., 1996; Arai et al., 1994, 1998; González-Jiménez et al., 2013). Such a model can explain why podiform chromitites have SSZ signatures. However, the universal existence of highly reduced and UHP minerals in the podiform chromitites is not consistent with this model (Yang et al., 1981; Bai et al., 2001, 2002, 2004, 2007; Yang et al., 2002, 2007, 2011, 2013, 2014, 2015a, b; Xu et al., 2008, 2009, 2013, 2015). Arai et al. (2013) proposed that the UHP chromitites were produced by deep recycling of low-P chromitites via mantle convection. They thought that the carbon-rich UHP minerals were changed from fluidal C species (e.g., CO_2) metasomatically entrapped during the travel of chromitites within the mantle. However, Yang et al. (2015) proposed that single element materials (such as C and H) were crystallized from the fluids released from previously

subducted slabs of continental and oceanic crust resting in the lower part of the mantle transition zone. These reduced minerals were carried by rising melts to the top of, or above, the transition zone and were encapsulated in high-pressure magnesiochromite (with dissolved Si). At the same time, minerals such as stishovite and qinsongite may have crystallized from the melts or fluids. With continued upwelling, coesite exsolution lamellaes formed in the chromite grains, and stishovite was replaced by coesite, but the diamonds were preserved as inclusions in magnesiochromite grains. They inferred that diamonds could occur in both MOR and back-arc basin (BAB) settings. Robinson et al. (2015) also suggested that as chromites were crystallized above the transition zone (400 km), highly reduced and UHP minerals that were stable at these depths could be captured. Thereafter, these chromites, along with peridotites, were brought by convective rise to shallow levels and were distributed widely in the upper oceanic mantle. Finally, they were mobilized by SSZ melts and fluids, and were redistributed to podiform chromitites containing diamonds and highly reduced minerals. Recently, Luo et al. (2018) pointed out that the formation of chromitites and shell dunites involved a large amount of deep fluids. In their model, the basic premise was continuous supply and rapid rise of deep fluids, which could prevent UHP and highly reduced phases entrained in deep fluids from oxidization and settlement during migration.

Zhao et al. (2019) reported the occurrence of clinopyroxene exsolution within chromite grains in the Cuobuzha chromitites, indicating that they have experienced a deep process in the mantle. In our study, the discovery of highly reduced minerals (e.g., Fe-Ni and Fe-Cr alloys) further confirms the deep origin of the Cuobuzha chromitites. We propose that these minerals were formed at the top of, or above, the transition zone and were incorporated into chromites. Then these chromites were carried by continued upwellings to the shallow mantle, during which clinopyroxene was exsolved from the chromite grains. However, the composition of chromites and the geochemistry of whole rock imply that the Cuobuzha chromitites have intimate affinities with boninites (Fig. 5–6, 9–10). Accordingly, we suggest that the Cuobuzha chromitites contain two types of chromites (high-pressure chromites and low-pressure chromites). The low-pressure chromites were formed through reaction between boninitic melts and peridotites, Meanwhile, the high-pressure chromites hosting highly reduced minerals were mobilized by melts and were reallocated to podiform chromitites.

7 Conclusions

(1) The Cuobuzha high-Cr chromitites are characterized by highly fractionated PGE pattern with low Pd/Ir ratios (<0.1), depletion in Al, Ga, V, Mg and Zn, and enrichment in Mn and Cr.

(2) The PGM assemblages indicate that $f(S_2)$ was initially low enough to allow the precipitation of Os-Fe alloy and then increased with reducing temperature.

(3) Calculated results show that parental magma of the Cuobuzha chromitites has an intimate boninitic affinity.

(4) As a model, we propose that the Cuobuzha chromitites contain high-pressure chromites and low-pressure chromites. Low-pressure chromites were formed through rock/melt reaction, during which the high-pressure chromites hosting highly reduced minerals were mobilized by melts and were reallocated to podiform chromitites.

References

Aitchison, J.C., Ali, J.R., and Davis, A.M., 2007. When and where did India and Asia collide? Journal of Geophysical Research, 112: 1–19.

Arai, S., and Abe, N., 1994. Podiform chromitite in the arc mantle: chromitite xenoliths from the Takashima alkali basalt, Southwest Japan arc. Mineralium Deposita, 29: 434–438.

Arai, S., 1997. Origin of podiform chromitites. Journal of Asian Earth Sciences, 15: 303–310.

Arai, S., and Matsukage, K., 1998. Petrology of a chromitite micropod from Hess Deep, equatorial Pacific: a comparison between abyssal and alpine-type podiform chromitites. Lithos, 43: 1–14.

Arai, S., and Miura, M., 2015. Podiform chromitites do form beneath mid-ocean ridges. Lithos, 232: 143–149.

Augé, T., 1988. Platinum-group minerals in the Tiebaghi and Vourinos ophilitic complexes; genetic implications. The Canadian Mineralogist, 26: 177–192.

Bai, W.J., Yang, J.S., Fang, Q.S., Yan, B.G., and Zhang, Z.M., 2001. Study on a storehouse of ultrahigh pressure mantle minerals— podiform chromite deposits. Earth Science Frontiers, 8: 111–121 (in Chinese with English abstract).

Bai, W.J., Shi, N.C., Yang, J.S., Fang, Q.S., Dai, M.Q., Xiong, M., and Yan, B.G., 2002. Two new varieties of iron nickel from ophiolites, Tibet. Acta Mineralogica Sinica, 22: 201–206 (in Chinese with English abstract).

Bai, W.J., Yang, J.S., Shi, N.C., Fang, Q.S., Dai, M.Q., Xiong, M., and Yan, B.G., 2004. A Discovery of Ultrahigh Pressure Minerals-Wustite and Native Iron from the Mantle Ophiolite, at Luobusa, Xizang. Geological Review, 50: 184–187 (in Chinese with English abstract).

Bai, W.J., Shi, N.C., Yang, J.S., Fang, Q.S., Ren, Y.F., Rong, H., Li, G.W., and Ma, Z.S., 2007. An Assemblage of Simple Oxide Minerals from Ophiolitic Podiform chromitites in Tibet and Their Ultrahigh Pressure Origin. Acta Geologica Sinica, 81: 1538–1549 (in Chinese with English abstract).

Ballhaus, C., and Sylvester, P., 2000. Noble metal enrichment processes in the Merensky Reef, Bushveld Complex. Journal of Petrology, 41: 545–561.

Bao, P.S., Wang, X.B., and Peng, G.Y., 1999. The Chromite Deposite in China. Beijing: Science Press, 98-142 (in Chinese with abstract).

Barnes, S.J., Boyd, R., Korneliussen, A., Nilsson, L.P., Often, M., Pedersen, R.B., and Robins, B., 1988. The use of mantle normalization and metal ratios in discriminating between the effects of partial melting, crystal fractionation and sulphide

segregation on platinum-group elements, gold, nickel and copper: Examples from Norway. In: Prichard, H.M. (ed.), Geo-Platinum Volume. Elsevier, 113–143.

Barnes, S.J., and Roeder, P.L., 2001. The Range of Spinel Compositions in Terrestrial Mafic and Ultramafic Rocks. Journal of Petrology, 42: 2279–2302.

Bédard, É., Hébert, R., and Guilmette, C., 2009. Petrology and geochemistry of the Saga and Sangsang ophiolitic massifs, Yarlung Zangbo Suture Zone, Southern Tibet: evidence for an arc-back-arc origin. Lithos, 113: 48–67.

Brenan, J.M., and Andrews, D.R.A., 2001. High-temperature stability of laurite and Ru-Os-Ir alloys and their role in PGE fractionation in mafic magmas. The Canadian Mineralogist, 39: 341–360.

Bockrath, C., Ballhaus, C., and Holzheid, A., 2004. Stabilities of laurite RuS2 and monosulphide liquid solution at magmatic temperature. Chemical Geololgy, 208: 265–271.

Cassard, D., Nicolas, A., Rabinovitch, M., Moutte, J., Leblanc, M., and Prinzhofer, A., 1981. Structural classification of chromite pods in southern New Caledonia. Economic Geology, 76(4): 805–831.

Constantinides, C.C., Kingston, G.A., and Fisher, P.C., 1980. The occurrence of platinum group minerals in chromitites of the Kokkinortsos chromite mine, Cyprus. In: Panayiotou, A. (ed.), Proc. Int. Ophiolite Symp. Ministry of Agriculture and Natural Resources, 93–101.

Dick, H.J.B., and Bullen, T., 1984. Chromium spinel as a petrogenetic indicator in abyssal and alpine-type peridotites and spatially associated lavas. Contributions to Mineralogy and Petrology, 86: 54–76.

Dickey, J.S., 1975. A hypothesis of origin for podiform chromite deposits. Geochimica et Cosmochimica Acta, 39: 1061–1074.

Dilek, Y., and Furnes, H., 2011. Ophiolite genesis and global tectonics: Geochemical and tectonic fingerprinting of ancient oceanic lithosphere. Geological Society of America Bulletin, 123: 387–411.

Dilek, Y., and Furnes, H., 2014. Ophiolites and Their Origins. Elements, 10: 93–100.

Distler, V.V., Kryachko, V.V., and Yudovskaya, M.A., 2008. Ore petrology of chromite-PGE mineralization in the Kempirsai ophiolite complex. Mineralogy & Petrology, 92: 31–58.

Edwards, S.J., Pearce, J.A., and Freeman, J., 2000. New insights concerning the influence of water during the formation of podiform chromite. In: Dilek, Y., Moores, E.M., Elthon, D., Nicolas, A. (eds.), Ophiolites and oceanic crust: new insights from field studies and the ocean drilling program, Boulder, Colorado. Geological Society of America Special Paper, 349.

Feng, G.Y., Yang, J.S., Xiong, F.H., Liu, F., Niu, X.L., Lian, D.Y., Wang, Y.P., and Zhao, Y.J., 2015. Petrology, geochemistry and genesis of the Cuobuzha peridotite in the western Yarlung Zangbo suture zone. Geology in China, 42: 1337–1353 (in Chinese with English abstract).

Feng, G.Y., Yang, J.S., Liu, S., Niu, X.L., Xiong, F.H., and Liu, F., 2016. Platinum-group element features of Cuobuzha peridotite from western Yarlung Zangbo suture zone. Acta Mineralogica Sinica, 36: 309–317 (in Chinese with English abstract).

Ferrario, A., and Garuti, G., 1990. Platium-group mineral inclusions in chromitites of the Finero mafic-ultramafic complex (lvrea-Zone, ltaly). Mineralogy & Petrology, 41: I25 – 143.

Frost, D.J., Liebske, C., Langenhorst, F., McCammon, C.A., Trønnes, R.G., and Rubie, D.C., 2004. Experimental evidence for the existence of iron-rich metal in the Earth's lower mantle. Nature, 428: 409–411.

Frost, D.J., and McCammon, C.A., 2008. The Redox state of Earth's mantle. Annual Review of Earth Planet Sciences, 36: 389–420.

Garuti, G., Zaccarini, F., and Moloshag, V., 1999. Platinum-group elements as indicators of sulphur fugacity in ophiolitic upper mantle: an example from chromitites of the Ray-Iz ultramafic complex, Polar Urals, Russia. The Canadian Mineralogist, 37: 1099–1115.

Gijbels, R.H., Millard, H.T., Deborough, G.A., and Bartel, A.J., 1974. Osmium, ruthenium, iridium and uranium in silicates and chromite from the eastern Bushveld Complex, South Africa.

Geochimica et Cosmochimica Acta, 38: 319–337.

Golubkova, A., Schmidt, M.W., and Connolly, J.A.D., 2016. Ultra-reducing conditions in average mantle peridotites and in podiform chromitites: a thermodynamic model for moissanite (SiC) formation. Contributions to Mineralogy & Petrology, 171:41.

Gonzalez-Jimenez, J.M., Marchesi, C., Griffin, W.L., Gutierrez-Narbona, R., Lorand, J.P., O'Reilly, S.Y., Garrido, C.J., Gervilla, F., Pearson, N.J., and Hidas, K., 2013. Transfer of Os isotopic signatures from peridotite to chromitite in the subcontinental mantle: insights from in situ analysis of platinum-group and base-metal minerals (Ojen peridotite massif, southern Spain). Lithos, 164–167, 74–85.

Hamlyn, P.R., Keays, R.R., Cameron, W.E., Crawford, A.J., and Waldron, H. M., 1985. Precious metals in magnesian low-Ti lavas: implications for metallogenesis and sulfur saturation in primary magmas. Geochimica et Cosmochimica Acta, 49: 1797 –1811.

Hébert, R., Bezard, R., Guilmette, C., Dostal, J., Wang, M., and Liu, Z.F., 2012. The Indus-Yarlung Zangbo ophiolites from Nanga Parbat to Namche Barwa syntaxes, southern Tibet: First synthesis of petrology, geochemistry, and geochronology with incidences on geodynamic reconstructions of Neo-Tethys. Gondwana Research, 22: 377–397.

Huang, G.C., Mo, X.X., Xu, D.M., Lei, Y.J., and Li, L.J., 2006. Origination and Evolution of Daba-Xiugugabu Ophiolite Belt in the Southwestern Tibet. Geology and Mineral Resources of South China, 3: 1–8 (in Chinese with English abstract).

Huang, G.C., Xu, D.M., and Lei, Y.J., 2007. Chromite prospects in the Daba-Xiugugabu ophiolite zone, southwestern Tibet. Geology in China, 34: 668–674(in Chinese with English abstract).

Irvine, T.N., 1967. Chromium spinels as a petrogenetic indicator. II, Petrologic applications. Canadian Journal of Earth Sciences, 4: 71–103.

Jaques, A.L., and Green, D.H., 1980. Anhydrous melting of peridotite at 0-15kb pressure and the genesis of tholeiitic basalts. Contributions to Mineralogy and Petrology, 73: 287–310.

Jin, Z.M., Bai, Q., and Kohlstedt, D.L., 1996. Experimental Study on the Relationship of Partial Melting in the Upper Mantle to Chromite Preconcentration. Geological Review, 42: 424–429 (in Chinese with English abstract).

Kamenetsky, V.S., Crawford, A.J., and Meffre, S., 2001. Factors controlling chemistry of magmatic spinel: an empirical study of associated olivine, Cr-spinel and melt inclusions from primitive rocks. Journal of Petrology, 42: 655–671.

Keays, R.R., 1995. The role of komatiitic and picritic magmatism and S-saturation in the formation of ore deposits. Lithos, 34: 1–18.

Kelemen, P.B., Joyce, D.B., Webster, J.D., and Holloway, J.R., 1990. Reaction between Ultramafic Rock and Fractionating Basaltic Magma Ⅱ. Experimental Investigation of Reaction between Olivine Tholeiite and Harzburgite at 1150-1050 ℃ and 5kb. Journal of Petrology, 31: 99–13.

Lago, L., Rabinowicz, M., and Nicolas, A., 1982. Podiform chromite ore bodies: A genetic model. Journal of Petrology, 23: 123–124.

Lauterbach, S., McCammon, C.A., Van, Aken. P., Langenhorst, F., and Seifert, F., 2000. Mössbauer and ELNES spectroscopy of (Mg,Fe)(Si,Al)O3 perovskite: a highly oxidised component of the lower mantle. Contributions to Mineralogy and Petrology, 138: 17–26.

Leblanc, M., and Nicolas, A., 1992. Ophiolitic chromitites. International Geological Review, 34: 653–686.

Li X.H., Wang, C.S., Li, Y.L., Wei, Y.S., and Chen, X., 2014. Definition and composition of the Zhongba Microterrane in southwest Tibet. Geological Bulletin of China, 88: 1372–1381 (in Chinese with English abstract).

Li, Y., Yang, J.S., Liu, Z., Jia, Y., and Xu, X., 2011. The origins of Baer ophiolitic peridotite and its implication in the Yarlung Zangbo suture zone, southern Tibet. Acta Petrologica Sinica, 27: 3239–3254 (in Chinese with English abstract).

Lian, D.Y., Yang, J.S. Xiong, F.H., Liu, F., and Wang, Y.P., 2015. Platinum group element characteristics of the peridotite and

podiform chromitite from Dajiweng ophiolite of the western segment of Yarlung-Zangbo suture zone, Tibet. Geology in China, 42: 525–546 (in Chinese with English abstract).

Liu, F., Yang, J.S., Chen, S.Y., Li, Z.L., Lian, D.Y., Zhou, W.D., and Zhang, L., 2013. Geochemistry and Sr-Nd-Pb isotopic composition of mafic rocks in the western part of Yarlung Zangbo suture zone: Evidence for intra-oceanic supra-subduction within the Neo-Tethys. Geology in China, 40: 742–755 (in Chinese with English abstract).

Liu, F., Yang, J.S., Dilek, Y., Xu, Z.Q., Xu, X.Z., Xiang, H., Chen, W., and Lian, D.Y., 2015a. Geochronology and geochemistry of basaltic lavas in the Dongbo and Purangophiolites of the Yarlung-Zangbo Suture zone: Plume-influenced continental margin-type oceanic lithosphere in southern Tibet. Gondwana Research, 27: 701–718.

Liu, F., Yang, J.S., Lian, D.Y., Zhao, H., Zhang, L., Zhang, L., and Huang, J., 2015b. The genesis and tectonic significance of mafic dikes in the Western part of the Yarlung Zangbo suture zone, Tibet. Acta Petrologica Sinica, 36: 441–454 (in Chinese with English abstract).

Locmelis, M., Pearson, N.J., Barnes, S.J., and Fiorentini, M.L., 2011. Ruthenium in komatiic chromite. Geochimica et Cosmochimica Acta, 75: 3645–3661.

Luo, Z.H., Jiang, X.M., Liu, X., Wu, Z.C., and Jing, W.C., 2018. Imprints of fluid process of shell dunite in ophiolitic chromite deposits: evidences from geology, petrology and crystal chemistry of olivine found in Luobusha and Zedang ophiolite in Yarlung Zangbo suture zone, Tibet. Earth Science Frontiers. 25: 1–14 (in Chinese with English abstract)

Maurel, C., and Maurel, P., 1982. Etude experimentale de la distribution de l'aluminium entre bain silicate basique et spinelle chromifere. Implications petrogenetiques: teneur en chrome des spinelles. Bulletin de Mineralogie, 105: 197–202.

Melcher, F., Grum, W., and Simon, G., 1997. Petrogenesis of the ophiolitic giant chromite deposits of Kempirsai, Kazakhstan: A study of solid and fluid inclusions in chromite. Journal of Petrology, 38: 1419–1458.

Nakagawa, M., and Franco, H.E.A., 1997. Placer Os-Ir-Ru alloys and sulfides: Indicators of sulfur fugacity in an ophiolite? The Canadian Mineralogist, 35: 1441–1452.

Naldrett, A.J., and Cabri, L.J., 1976. Ultramafic and related mafics rocks: their classification and genesis with special reference to the concentration of nickel sulfides and platinum-group elements. Economic Geology, 71: 1131–1158.

Nicolas, A., 1989. Structures of Ophiolite and Dynamics of Oceanic Lithosphere. Doedrecht: Kluwer Academic Publishers, 223–252

Pagé, P., and Barnes, S.J., 2009. Using Trace Elements in Chromites to Constrain the Origin of Podiform Chromitites in the Thetford Mines Ophiolite, Quebec, Canada. Economic Geology, 104: 997–1018.

Pagé, P., Barnes, S.J., Bédard, J.H., and Zientek, M.L., 2012. In situ determination of Os, Ir, and Ru in chromites formed from komatiite, tholeiite and boninite magmas: implications for chromite control of Os, Ir and Ru during partial melting and crystal fractionation. Chemical Geology, 302–303, 3–15.

Pan, G.T., Chen, Z.L., and Li, X.Z., 1997. The Formation and Evolution of the East Tethyan. Beijing: Geological Publishing House, 100 (in Chinese).

Pearce, J.A., Lippard, S.J., and Roberts, S., 1984. Characteristics and tectonic significance of supra-subduction zone ophiolites. In: Kokelaar, B.P, and Howells, M.F. (eds.), Marginal basin geology. Geological Society of London Special Publication, Blackwell Scientific Publications, 16: 77–94

Robinson, P.T., Trumbull, R.B., Schmitt, A., Yang, J.S., Li, J.W., Zhou, M.F., Erzinger, J., Dare, S., and Xiong, F.H., 2015. The origin and significance of crustal minerals in ophiolitic chromitites and peridotites. Gondwana Research, 27: 486–506.

Rollinson, H., and Adetunji, J., 2013. Mantle podiform chromitites do not form beneath mid-ocean ridges: A case study from the Moho transition zone of the Oman ophiolite. Lithos, 177: 314–327.

Rollinson, H., 2008. The geochemistry of mantle chromitites from the northern part of the Oman ophiolite: inferred parental melt compositions. Contributions to Mineralogy and Petrology, 156: 273–288.

Sattari, P., Brenan, J.M., Horn, I., McDonough, W.F., 2002. Experimental constraints on the sulphide- and chromite–silicate melt partitioning behaviour of rhenium and platinum-group elements. Economic Geology, 97: 385–398.

Stockman, H.W., and Hlava, P.F., 1984. Platinum-group minerals in alpine chromitites from Southwestern Oregon. Economic Geology, 79: 491–508.

Sun, S.S., Wallace, D.A., Hoatson, D.M., Glikson, A.Y., Keays, R.R., 1991. Use of geochemistry as a guide to platinum group element potential of mafic-ultramafic rocks: Examples from the west Pilbara Block and Halls Creek Mobile Zone, Western Australia. Precambrian Research, 50: 1–35.

Sun, M., Jain, J., Zhou, M.F., and Kerrich, R.A., 1993. procedural modification for enhanced recovery of precious metals, gold, PGE) following nickel sulfide fire assay and tellurium coprecipitation: Applications for analysis of geological samples by Inductively Coupled Plasma Mass Spectrometry. Canadian Journal of Applied Spectroscopy, 38: 103–108.

Thayer, T.P., 1964. Principal features and origin of podiform chromite deposits, and some observations on the Gulemen-Soridag district, Turkey. Economic Geology, 59: 1497–1524.

Tian, Y.Z., Yang, J.S., Yang, H.S., Tian, Y.L., 2019. The characteristics of PGM and BMS in Sartohay chromitites, Xinjiang. Acta Geologica Sinica, 93: 2639–2655.

Tredoux, M., Lindsay, N.M., avies, G., and MacDonald, I., 1995. The fractionation of platinum-group elements in magmatic systems, with the suggestion of a novel causal mechanism. South African Journal of Geology, 98: 157–167.

Wang, X.B., Hao, Z.G., and Bao, P.S., 1992. Genetic types and some metallogenic characteristics of chromite deposits in ophiolites within phanerozoic orogenic belts of China. Mineral deposits, 11: 23-36 (in Chinese with English abstract).

Woodland, A.B., and Koch, M., 2003. Variation in oxygen fugacity with depth in the upper mantle beneath the Kaapvaal craton, Southern Africa. Earth and Planetary Science Letters, 214: 295–310.

Xia, B., Zheng, R., Hong, Y.R. Zhou, X., Cao, Y.G., 1997. The lithogeochemical characteristics and origin of Dajiweng ophiolite in Xizang (Tibet). Earth and Environment, 1: 46–52 (in Chinese with English abstract).

Xia, B., and He, P.Y., 1995. Petrogeochemistry and genetic significance of the Jianapeng ophiolite, Tibet. Acta Mineralogica Sinica, 15: 236–242 (in Chinese with English abstract).

Xu, D.M., Huang, G.C., Huang, L.Q., Lei, Y.J., and Li, L.J., 2006. The Origin of Mantle Peridotites in the Daba-Xiugugabu Ophiolite Belt, SW Tibet. Geology and Mineral Resources of South China, 3: 10–18 (in Chinese with English abstract).

Xu, D.M., Huang, G.C., and Lei, Y.J., 2007. Origin of the Xiugugabu ophiolite massif, SW Tibet: Evidence from petrology and geochemistry. Geotectonica et Metallogenia, 31: 490–501 (in Chinese with English abstract).

Xu, X.Z., Yang, J.S., Ba, D.Z., Chen, S.Y., Fang, Q.S., and Bai, W.J., 2008. Diamond discovered from the Kangjinla chromitite in the Yarlung Zangbo ophiolite belt, Tibet. Acta Petrologica Sinica, 24: 1453–1462 (in Chinese with English abstract).

Xu, X.Z., Yang, J.S., Guo, G.L., and Li, J.Y., 2011. Lithological research on the Purang mantle peridotite in western Yarlung-Zangbo suture zone in Tibet. Acta Petrologica Sinica, 27: 3179–3196 (in Chinese with English abstract).

Xu, X.Z., Yang, J.Z., Chen, S.Y., Fang, Q.S., Bai, W.J., and Ba, D.Z., 2009. Unusual mantle mineral group from chromitite orebody Cr-11 in Luobusa ophiolite of Yarlung-Zangbo suture zone, Tibet. Journal of Earth Science (English Edition), 20: 284–302.

Xu, X.Z., Yang, J.S., Guo, G.L., and Xiong, F.H., 2013. Mineral inclusions in corundum from chromitites in the Kangjinla chromite deposi, Tibet. Acta Petrologica Sinica, 29: 1867–1877 (in Chinese with English abstract).

Xu, X.Z., Yang, J.S., Robinson, P.T., Xiong, F.H., Ba, D.Z., and Guo, G.L., 2015. Origin of ultrahigh pressure and highly reduced minerals in podiform chromitites and associated mantle peridotites of the Luobusa ophiolite, Tibet. Gondwana Research, 27: 686–700.

Xiong, F.H., Yang, J.S., Liang, F.H., Ba, D.Z., Zhang, J., Xu, X.Z., Li, Y., and Liu, Z., 2011. Zircon U-Pb ages of the Dongbo ophiolite in the western Yarlung Zangbo Suture Zone and their geological significance. Acta Petrologica Sinica, 27: 3223–3238 (in Chinese with English abstract).

Xiong, F.H., Yang, J.S., Robinson, P.T., Xu, X.Z., Liu, Z., Li, Y., Li, J.Y., and Chen, S.Y., 2014. Origin of Podiform Chromitite, a New Model Based on the Luobusa Ophiolite, Tibet. Gondwana Research, 27: 525–542.

Xiong, F.H., Yang, J.S., Robinson, P.T., Xu, X.Z., Ba, D.Z., Li, Y.,and Zhang, Z.M., 2016. Diamonds and Other Exotic Minerals Recovered from Peridotites of the Dangqiong Ophiolite, Western Yarlung Zangbo Suture Zone, Tibet. Acta Geologica Sinica (English Edition), 90(2): 425–439.

Xiong, F.H., Yang J.S., Robinson P.T., Dilek Y., Milushi I., Xu X.Z., Zhou W.D., Zhang Z.M., and Rong H., 2017. Diamonds discovered from High-Cr podiform chromitites of Bulqiza, Eastern Mirdita Ophiolite (EMO), Albania. Acta Geologica Sinica (English Edition), 91(2): 455–468.

Yamamoto, S., Komiya, T., Hirose, K., and Maruyama, S., 2009. Coesite and clinopyroxene exsolution lamellae in chromites: In-situ ultrahigh-pressure evidence from podiform chromitites in the Luobusa ophiolite, southern Tibet. Lithos, 109: 314-322.

Yang, J., 2015b. Diamond-bearing Ophiolites and Their Geological Occurrence. Episodes, 38: 344–364.

Yang, F.Y., Kang, Z.Q., and Liu, S.C., 1981. A new octahedral pseudomorph of lizardite and its origin. Acta Mineralogica Sinica, 1: 52–54 (in Chinese with English abstract).

Yang, J.S., Bai, W.J., Fang, Q.S., Yan, B.G., Shi, N.C., Ma, Z.S., Dai, M.Q., and Xiong, M., 2002. Silicon-rutile-an ultrahigh pressure (UHP) mineral from an ophiolite. Progress in National Science, 13: 528–531 (in Chinese).

Yang, J.S., Dobrzhinetskaya, L., Bai, W.J., Fang, Q.S., Robinson, P.T., Zhang, J.F., and Green, H.W., 2007. Diamond-and coesite-bearing chromitites from the Luobusa ophiolite, Tibet. Geology, 35: 875–878.

Yang, J.S., Xu, X.Z., Li, Y., Li, J.Y., Ba, D.Z., Rong, H., and Zhang, Z.M., 2011. Diamonds recovered from peridotite of the Purang ophiolite in the Yarlung Zangbo suture of Tibet: A proposal for a new type of diamond occurrence. Acta Petrologica Sinica, 27: 3171–3178 (in Chinese with English abstract).

Yang, J.S., Xu, X.Z., Zhang, Z.M., Rong, H., Li, Y., Xiong, F.H., Liang, F.H., Liu, Z., Liu, F., Li, J.Y., Li, Z.L., Chen, S.Y., Guo, G.L., and Robinson, P., 2013. Ophiolite-type diamond and deep genesis of chromitite. Acta Geoscientica Sinica, 34: 643–653 (in Chinese with English abstract).

Yang, J. S., Robinson, P.T., and Dilek, Y., 2014. Diamonds in ophiolites. Elements, 10: 127–130.

Yang, J.S., Meng, F. C., Xu, X.Z., Robinson, P.T., Dilek, Y., Makeyev, A.B., Wirth, R., Wiedenbeck, M., and Cliff, J., 2015a. Diamonds, native elements and metal alloys from chromitites of the Ray-Iz ophiolite of the Polar Urals. Gondwana Research, 27: 459–485.

Yang, J.S., Xiong, F.H., Guo, G.L., Liu, F., Liang, F.H., Chen, S.Y., Li, Z.L., and Zhang, L.W., 2011. The Dongbo ultramafic massif: A mantle peridotite in the western part of the Yarlung Zangbo suture zone, Tibet, with excellent prospects for a major chromite deposit. Acta Petrologica Sinica, 27: 3207–3222 (in Chinese with English abstract).

Yin, A., and Harrison, T.M., 2000. Geologic evolution of the Himalayan Tibetan orogen. Annual Review of Earth Planet Sciences, 28: 211–280.

Zhang, W.P., Yuan, S.H., and Liu, W., 2011. Distribution and Research Significance of Ophiolite in Brahmaputra Suture Zone, Southern Tibet. Northwestern Geology, 44:1–9 (in Chinese with English abstract).

Zhao, H., Yang, J.S., Liu, F., Xiong, F.H., Lian, D.Y., Yao, H., and Dong, Y.F., 2019. Features of the Cuobuzha podiform chromitite along western Yarlung Zangbo suture zone in Tibet: Implications for its tectonic setting. Geology in China, 46: 115–125(in Chinese with English abstract).

Zhou, M.F., Robinson, P.T., Su, B.X., Gao, J.F., Li, J.W., Yang, J.S., and Malpas, J., 2014. Compositions of chromite, associated minerals, and parental magmas of podiform chromite deposits: The role of slab contamination of asthenospheric melts in suprasubduction zone environments. Gondwana. Research, 26: 262–283.

Zhou, M.F., and Robinson, P.T., 1994. High-Cr and high-Al podiform chromitites, Western China: relationship to partial melting and melt/rock reaction in the upper mantle. International geology review, 36: 678–686.

Zhou, M.F., Robinson, P.T., Malpas, J., and Li, Z.J., 1996. Podiform chromitites in the Luobusa ophiolite (Southern Tibet): implications for melt-rock interaction and chromite segregation in the upper mantle. Journal of Petrology, 37: 3–21.

Zhou, M.F., and Robinson, P.T., 1997. Origin and tectonic environment of podiform chromite deposits. Economic Geology, 92: 259–262.

Zhou, M.F., Sun, M., Keays, R.R., Kerrich, R.W., 1998. Controls on platinum-group elemental distributions of podiform chromitites: a case study of high-Cr and high-Al chromitites from Chinese orogenic belts. Geochimica et Cosmochimica Acta, 62: 677–688.

Zhou, M.F., Robinson, P.T., Malpas, J., Edwards, S.J., and Qi, L., 2005. REE and PGE geochemical constraints on the formation of dunites in the Luobusa ophiolite, southern Tibet. Journal of Petrology, 46: 615–639.

About the first author

ZHAO Hui, female, born in 1992 in Qujing City, Yunnan Province; doctoral student in Harbin Institute of Technology; She is now interested in the study on petrogenesis of igneous rocks and non-traditional isotopes; Email:13717926721 @163.com; phone: 13717926721.

About the corresponding author

YANG Jingsui, male, born in 1950 in Hangzhou City, Zhejiang Province; doctor; graduated from Dalhousie University in Canada; Professor at the Institute of Geology, Chinese Academy of Geological Sciences, Beijing, China. He has been working on ultra-high pressure (UHP) metamorphic belts in China, and ophiolites in different orogenic belts around the world. Email:yangjsui@163.com; phone: 010-68999698.